



ORIGINAL ARTICLE

Novel supercapacitor electrodes based semiconductor nanoheterostructure of CdS/rGO/CeO₂ as efficient candidates

Asma A. Ali ^a, Ahmed Abdel Nazeer ^b, Metwally Madkour ^b, Ali Bumajdad ^{b,*}, Fakhreia Al Sagheer ^{b,*}

^a Science Department, College of Basic Education, Public Authority of Applied Education and Training (PAAET), P.O. Box 23167, Safat 13092, Kuwait

^b Chemistry Department, Faculty of Science, Kuwait University, P.O. Box 5969, Safat 13060, Kuwait

Received 3 December 2017; accepted 10 March 2018

Available online 19 March 2018

KEYWORDS

Nanoheterostructure;
Semiconductors;
Galvanostatic charge-discharge;
Specific capacitance

Abstract In this study, we have synthesized metal oxide/metal sulphide based nanoheterostructures mediated with graphene nanosheets. The synthesized nanoheterostructures were characterized via different techniques such as XRD, XPS, and TEM. The electrochemical characteristics of the investigated nanoheterostructure (CdS/rGO/CeO₂) were investigated through electrochemical impedance spectroscopy (EIS), cyclic voltammetry (CV), and galvanostatic charge-discharge. The specific capacitance of the single rGO, binary CdS/CeO₂ and ternary CdS/rGO/CeO₂ heterostructures were measured. The CdS/rGO/CeO₂ nanoheterostructure showed the most excellent cycling stability with high specific capacitance of 407 F g⁻¹ achieved at a charge-discharge rate of 1 A/g. The investigated supercapacitor retained about 96% of the initial energy density after charge-discharge at a 10 A/g for 5000 cycles. The ternary CdS/rGO/CeO₂ nanoheterostructure revealed the best specific capacitance as the graphene nanosheets increased interfacial electron transfer. The results revealed that the investigated novel nanoheterostructure is among the best reported ones in the literature.

© 2018 The Authors. Production and hosting by Elsevier B.V. on behalf of King Saud University. This is an open access article under the CC BY-NC-ND license (<http://creativecommons.org/licenses/by-nc-nd/4.0/>).

1. Introduction

It is of great importance to develop a new non-polluting (environmentally friendly) renewable energy source and energy storage systems to overcome the fossil fuels related problems and the energy demand. One of the most important energy storage systems recently used are the supercapacitors which known also as ultracapacitors or electrochemical capacitors that can provide large amounts of energy in short time to be used in different important applications (Miller and Simon,

* Corresponding authors.

E-mail addresses: a.bumajdad@ku.edu.kw (A. Bumajdad), f.alsagheer@ku.edu.kw (F. Al Sagheer).

Peer review under responsibility of King Saud University.



Production and hosting by Elsevier

2008). The main advantages of using supercapacitors are their fast charging-discharging process, high power density, long cycle life, and the ability to use in wide range of temperatures. Carbonaceous based supercapacitors which have high electrical conductivity, surface area and porosity showed high power density and energy (Frackowiak, 2007). Carbonaceous materials including carbon nanotubes (CNT), fullerenes and graphene (rGO) have remarkable and unique chemical, physical, and electronic characteristics that make them attractive for next generation miscellaneous field of research such as supercapacitors, electronics, batteries, fuel cells, electrochemical sensors, biosensors, and medicinal applications (Li et al., 2012). Once discovered in 2004, Graphene has attracted a great attention owing to its exceptional thermal, mechanical and optoelectronic characteristics. Graphene exhibits excellent charge carrier mobility and a large surface area, which enables it to be a targeted candidate to be used as an electron mediator to accomplish efficient charge separation in electron transfer processes (Wang et al., 2013). Graphene-based supercapacitors offer good flexibility and thermal stability (Li et al., 2013). To enhance the specific capacitance and the electrochemical properties of the prepared graphene based supercapacitors, different strategies was investigated by researchers including studying ternary composites to be uses as supercapacitors (Sankar and Selvan, 2015; Han et al., 2014). The fabrication of a heterostructure is an effectual approach to enhance the electrical activity because of the blend of merits of each component (Han et al., 2014). In the heterostructure; graphene could acts as an excellent electron mediator and a gap linker to improve the charge separation efficiency (Wang et al., 2010).

Also, metal oxides have been widely used for application in supercapacitors due to their different oxidation states for pseudocapacitance generation (Huang et al., 2015). From these metal oxides, MnO_2 , RuO_2 and IrO_2 have been widely studied as redox supercapacitor candidates depending on their high pseudocapacitance resulted from their fast redox reactions (Xue et al., 2007). The most important one is RuO_2 but its toxicity, high cost and abundance limit its use in different applications (Chen et al., 2004). Cerium oxide, Ceria, (CeO_2), as one of the rare earth metal oxides, with a wide band gap ($E_g = 3.15$ eV), has attracted extreme significance. Ceria has the fluorite structure, which is stable from room temperature till melting point. It plays an essential role in environmental and energy correlated applications, such as solar cells, catalysis, capacitors and fluorescence (Bumajdad et al., 2009). CeO_2 is considered as good alternative to be used due to its abundance, environmental safe, low cost and excellent electrochemical redox properties (Bumajdad et al., 2006; Kalubarme et al., 2013). Moreover, the cerium oxidation state can change quickly between III and IV which facilitate its application as superconductors (Su et al., 2013). The main problem of using metal oxides is their poor electrical conductivity which makes their surface part only contribute in the total capacitance while the other interior parts are difficult to contribute in the charge storage process which decreases the total performance of the supercapacitors. Also using carbonaceous ternary nanocomposites was one of the effective strategies to solve this problem. On contrast, CdS semiconductor nanoparticles have excellent electrical, physical and optical properties, which make it a good candidate for wide range of applications such as solar cells, electrochemical biosensor, light detectors, photocatalysis

and supercapacitors (Zhang and Zhu, 2010; Cao et al., 2010; Yang et al., 2010). Zhang et al., studied CdS nanoparticles with 3D rGO which exhibited a high specific capacitance of 300 F/g at a scan rate 5 mV/s, which confirms the possibility of 3D rGO/CdS architecture to be used in energy storage applications (Zhang et al., 2016).

In this study, a nanoheterostructure based on metal oxide/metal sulphide semiconductors mediated with rGO nanosheets have been synthesized. To best of our knowledge, this nanoheterostructure has not been ever studied. Moreover, the pseudocapacitive performance of single rGO, binary CdS/ CeO_2 and ternary CdS/rGO/ CeO_2 heterostructures in 2 M KOH has been investigated and reported. The ternary CdS/rGO/ CeO_2 nanoheterostructure revealed the best specific capacitance as the graphene nanosheets increased interfacial electron transfer. The results revealed that the investigated novel nanoheterostructure is among the best reported materials in the literature.

2. Experimental

2.1. Materials

All chemicals (cerium(III)nitrate hexahydrate, sodium hydroxide, sodium nitrate, graphite powder, sulphuric acid, potassium permanganate, hydrazine hydrate, hydrogen peroxide, sodium sulphide, polyvinylalcohol, polyvinyl pyrrolidone, cadmium nitrate) and solvents (ethanol and acetone) were of analytical grade (Sigma-Aldrich) and were used as received without any further purification.

2.2. Synthesis of nanoparticles

2.2.1. Preparation of graphene oxide

Graphene oxide was prepared according to the modified Hummer's method (Hummers and Offeman, 1958; Liang et al., 2011) in which 2.0 g of graphite powder was added into a 250 ml beaker, followed by the addition of 1.0 g sodium nitrate NaNO_3 and 46 ml H_2SO_4 into it sequentially under stirring in an ice-bath at 0 °C. Then KMnO_4 (6.0 g) was added slowly into the beaker under stirring and control the temperature below 20 °C. The ice-bath was removed after 5.0 min and heated at 35 °C for 30 min, then 92 ml D.I H_2O was added slowly into the system and the temperature increased up to 98 °C and stirring was continued for another 30 min. Then 280 ml hot water with 60 °C and 30% Hydrogen peroxide, H_2O_2 , (30 ml) aqueous solution were added to reduce the residual KMnO_4 till no bubble was appeared. Finally, the system was centrifuged at 7200 rpm for 10 min, and the obtained powder was washed by warm water until the initially black colored mixture changes into a reddish-brown color. For preparation of graphene, 0.1 g of the prepared GO was sonicated in 20 ml deionized water until obtaining a homogeneous yellow dispersion. 100 ml of hydrazine hydrate was added as reducing agent into the solution and transferred inside a conventional microwave. The microwave oven was operated at a full power (1000 W) in 30 s cycles (on for 10 s, off for 20 s) for a total reaction time of 60 s. The yellow color of GO was changed to a black color indicating complete reduction to graphene.

2.2.2. Synthesis of CdS quantum dots nanoparticles

The CdS QDs were prepared by adding 0.2 M cadmium nitrate to a 5% aqueous solution of PVA/PVP (50:50, %wt) under continuous stirring. After that, an equal volume of 0.2 M sodium sulphide was added dropwise to the solution with continuous stirring. Then, the solution was transferred to a 100 ml Teflon-lined stainless steel autoclave inside an oven at 110 °C for 5 h. Finally, the product was washed three times with distilled water then centrifuged at a speed of 8000 rpm. The obtained yellow precipitate of CdS QDs was dried overnight in a vacuum oven at 40 °C.

2.2.3. Synthesis of CeO₂ nanoparticles

CeO₂ nanoparticles were prepared by a modified precipitation method. In a typical procedure, a 0.03 M of Ce(NO₃)₃·6H₂O was dissolved in distilled water. Then, this solution was transferred portion wise to a beaker containing 100 ml of NaOH solution with a constant pH value of 13. A precipitate was formed, washed with distilled water, then centrifuged at a speed of 8000 rpm for 10 min. The washed precipitate was dried overnight in a vacuum oven at 40 °C.

2.2.4. Synthesis of rGO/CdS heterostructured nanoparticles

To a 5% aqueous solution of PVA/PVP (50:50, %wt), 2% rGO suspension (v/v) (6 mg) was added and the solution allowed stirring. rGO/CdS NPs were prepared by adding certain volume of 0.2 M cadmium nitrate to the prepared solution under continuous stirring. After that, certain volume of 0.2 M sodium sulphide was added dropwise to the solution under continuous stirring. Then, the solution mixture was transferred to a 100 ml Teflon-lined stainless steel autoclave inside an oven at 110 °C for 5 h. Finally, the product was washed three times with distilled water then centrifuged at a speed of 8000 rpm. The obtained precipitate of rGO/CdS NPs was dried overnight in a vacuum oven at 40 °C.

2.2.5. Synthesis of hybrid heterostructures of CdS/CeO₂ and CdS/rGO/CeO₂

Firstly, 0.03 M of Ce(NO₃)₃·6H₂O was dissolved in a dispersion of CdS and CdS/rGO suspensions (0.45 g for each) with stoichiometric amounts in order to obtain CdS/CeO₂ and CdS/rGO/CeO₂ heterostructures with 1:2 and 1:0.01:2 respectively. Then, this solution was transferred to a beaker containing 100 ml of NaOH solution. The pH value of the solutions during experiment should maintained constant to around 13. A precipitate was formed, washed with distilled water, then centrifuged at a speed of 8000 rpm for 10 min. The washed precipitate was dried overnight in a vacuum oven at 40 °C.

2.3. Characterization

The X-ray powder diffraction (XRD) analysis was conducted using D8 Advance diffractometer with a copper target and nickel filter with CuK α radiation ($\lambda = 0.154056$ nm). The shape of the nanoparticles was investigated using transmission electron microscopy (TEM) using a JEOL JEM 1230 operating at 120 kV. X-ray photoelectron spectroscopy (XPS) measurements were conducted using Thermo ESCA Lab 250xi equipped with Mg K α radiation (1253 eV).

2.4. Electrochemical measurements

Potentiostat/Galvanostat model Gamry 3000 was used for electrochemical measurements such as cyclic voltammetry (CV), electrochemical impedance spectroscopy (EIS) and galvanostatic charge-discharge. Glassy carbon electrode coated with the investigated CdS/rGO/CeO₂ nanoheterostructure was used as working electrode. Also, saturated calomel electrode and platinum foil were used as reference and counter electrodes, respectively. 2 M KOH solution was used as electrolyte. Electrochemical impedance spectroscopy measurements were conducted at $E_{app} = 0.0$ V with ac voltage of 5 mV in the frequency range from 0.01 Hz to 100 kHz. Echem analyst software was used for data analysis. For preparing the working electrode, mixture of 2 mg of CdS/rGO/CeO₂ powder in 700 μ L isopropyl alcohol with 6 μ L Nafion was vigorously sonicated for 2 h. Then the working electrode was prepared by drop casting of 10 μ L of the mixture onto glassy carbon electrode.

3. Results and discussion

3.1. Characterization of nanoparticles

X-ray photoelectron spectroscopy (XPS) spectra of the prepared CdS/rGO/CeO₂ nanoheterostructure Fig. 1 indicates the presence of Cd, S, O, Ce, and C signals. The binding energy of peaks corresponding to Cd 3d_{5/2} and Cd 3d_{3/2} peaks for CdS are observed at 405.5 eV and 412.2 eV in Fig. 1A (Zhao et al., 2010). The two obvious peaks observed at 161.7 eV and 162.9 eV in Fig. 1B correspond to the characteristic S 2p_{3/2} and S 2p_{1/2} peaks of S²⁻ for CdS NPs (Jing and Guo, 2007). The C1s spectrum of rGO sheets shown in Fig. 1C reveals a sharp peak at 284.5 eV that corresponds to C—C bonds of carbon atoms in the honeycomb lattice. Peaks at 285.6, and 287.7 eV could be assigned to different C—O bonding configurations due to the harsh oxidation which destroyed the sp² atomic structure of graphite (Some et al., 2012).

The O 1s spectrum in Fig. 1D showed three peaks at 529.1 eV, 531.9 eV and 533.7 eV. The shoulder appeared at 531.9 eV was assigned to the adsorbed oxygen and weakly bonded oxygen species. The peak at 533.7 eV is belonged to oxygen from hydroxide or adsorbed water on the catalyst surface. Both peaks confirmed the existence of surface oxygen vacancies in CeO₂. However, the weakest peak, located at 529.1 eV, was attributed to lattice oxygen in the anchored CeO₂ nanocrystals (Wang et al., 2011; Wang et al., 2013; Shan et al., 2012). Generally, surface adsorbed oxygen is more reactive than lattice oxygen in oxidation reactions because of its higher mobility (Shan et al., 2012). Regarding the Ce 3d spectrum Fig. 1E, the six peaks observed and denoted as (882.5 eV), (889.3 eV), (898.5 eV), (901.0 eV), (907.5 eV) and (916.8 eV), can be assigned to Ce 3d of CeO₂, which are identical with the reported values (Primo et al., 2011; Yang et al., 2014).

Fig. 2 presents the typical XRD patterns of the as-prepared rGO, CeO₂, CdS, CdS/CeO₂ and CdS/rGO/CeO₂ nanoheterostructures. Diffraction peaks of the bare CeO₂ at 28.8°, 33.3°, 47.6° and 56.4° can be indexed as the (1 1 1), (2 0 0), (2 2 0) and (3 1 1) planes of the face-centered cubic structure of CeO₂ (JCPDS No. 34-0394), respectively (You et al., 2016). And the peaks of the bare CdS at 26.5°, 44.0° and 52°

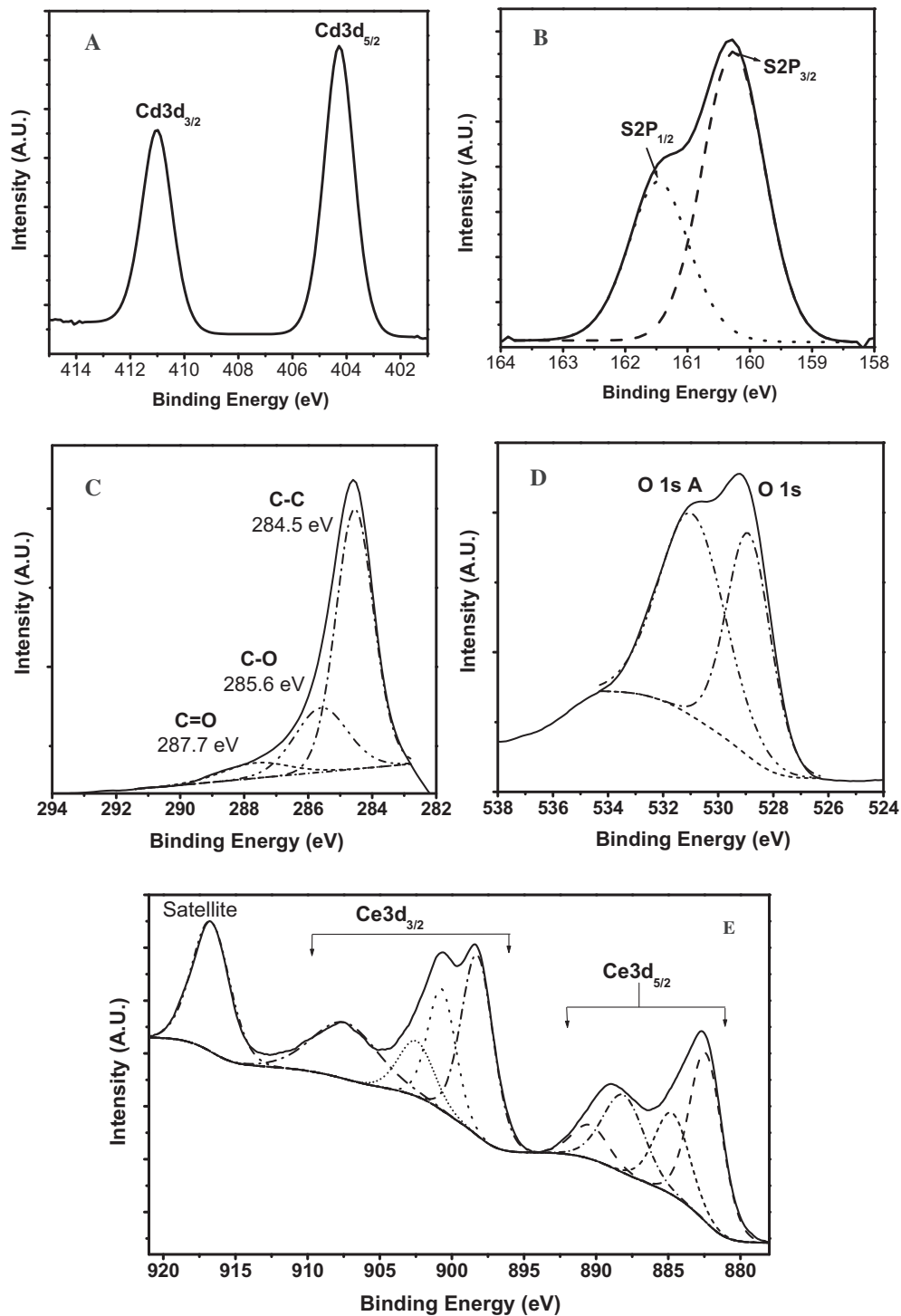


Fig. 1 XPS spectra for Cd 3d, S 2p, C 1s, O 1s and Ce 3d for CdS/rGO/CeO₂ nanoheterostructure.

can be characterized as the (1 1 1), (2 2 0) and (3 1 1) planes of the cubic structure of CdS (JCPDS No.42-1411), respectively (You et al., 2016). The crystallite sizes of the synthesized nanoheterostructures were calculated using the Debye-Scherrer equation Eq. (1):

$$D = 0.89\lambda / (\beta \cos \theta) \quad (1)$$

where λ is the wavelength (Cu K α), β is the full width at half-maximum and θ is the diffraction angle obtained from 2θ values corresponding to the most intense peak in XRD pattern (1 1 1). The calculated average crystallite sizes were found to be ~ 3.4 and ~ 2.5 nm for bare CeO₂ and CdS nanoparticles respectively. The broad peak at 24.67° indicates a random pucking of graphene sheets in the rGO. This peak is

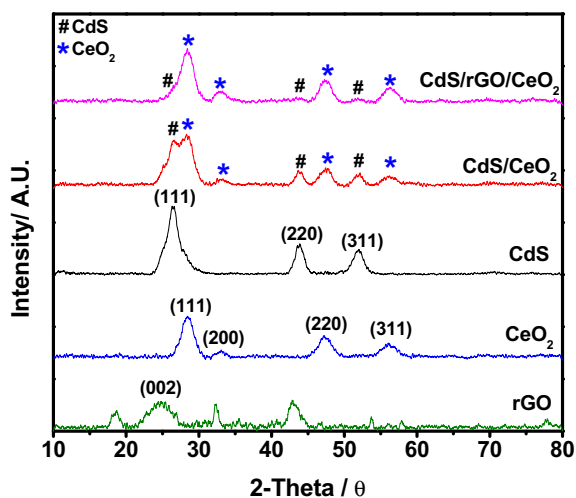


Fig. 2 XRD patterns of the as-prepared rGO, CeO₂, CdS, CdS/CeO₂ and CdS/rGO/CeO₂ nanoheterostructure.

corresponding to (0 0 2) plane of graphite and this confirms the reduction process of graphene oxide to graphene (Kumar et al., 2016). The XRD pattern of the CdS/CeO₂ nanoheterostructure exhibit the characteristic diffraction peaks of both CdS and CeO₂ phases, indicating the presence of CeO₂ and CdS with ratios of 67.6%: 32.4% respectively. The XRD pattern of the CdS/rGO/CeO₂ nanoheterostructure clearly exhibit the characteristic peaks of CeO₂ while the peaks for CdS are very weak with slight variations in peak parameters in terms of broadening and intensity. This behavior of

CdS/rGO/CeO₂ nanoheterostructure pattern is expected due to the composition ratios 1:0.01:2 which interpret the weak appearance of CdS peaks and the disappearance of rGO peaks and this phenomenon is matched with previously reported data (Kumar et al., 2016).

To have better insight on the morphology, TEM analysis was carried out. From TEM images, non-aggregated and well dispersed spherical nanoparticles were obtained for CdS and CeO₂ nanoparticles. From Fig. 3B, it can be found that the CeO₂ NPs with an average diameter around 3.9 nm. As shown in Fig. 3C, the highly ordered CdS QDs displayed an average diameter of about 3.4 nm. Fig. 3D shows a typical TEM image of CdS/CeO₂ heterostructure which showed homogeneous distribution of the heterostructure with an average particle size of 4.8 nm which is most likely resulted from the adjacent contact of CdS and CeO₂ nanoparticles. The CdS/CeO₂ heterostructures are seen along with smooth rGO sheets as shown in Fig. 3E and F.

3.2. Electrochemical performance

The electrochemical behavior of rGO, CdS/CeO₂ and CdS/rGO/CeO₂ nanoheterostructures was studied by cyclic voltammetry (CV) measurements in 2 M KOH aqueous electrolyte in a potential window of 0–1 V at a scanning rate of 10 mV s⁻¹ as shown in Fig. 4A. The cyclic voltammetric curve of rGO features perfect rectangular and symmetric shaped curve, indicative of the perfect electrical double-layer capacitance behavior (Chen et al., 2012). In case of CdS/rGO/CeO₂ the CV curve shows a remarkable increase in the current density and the electrochemical area compared with CdS/CeO₂. Introducing the reduced graphene oxide to CdS/CeO₂ pronouncedly

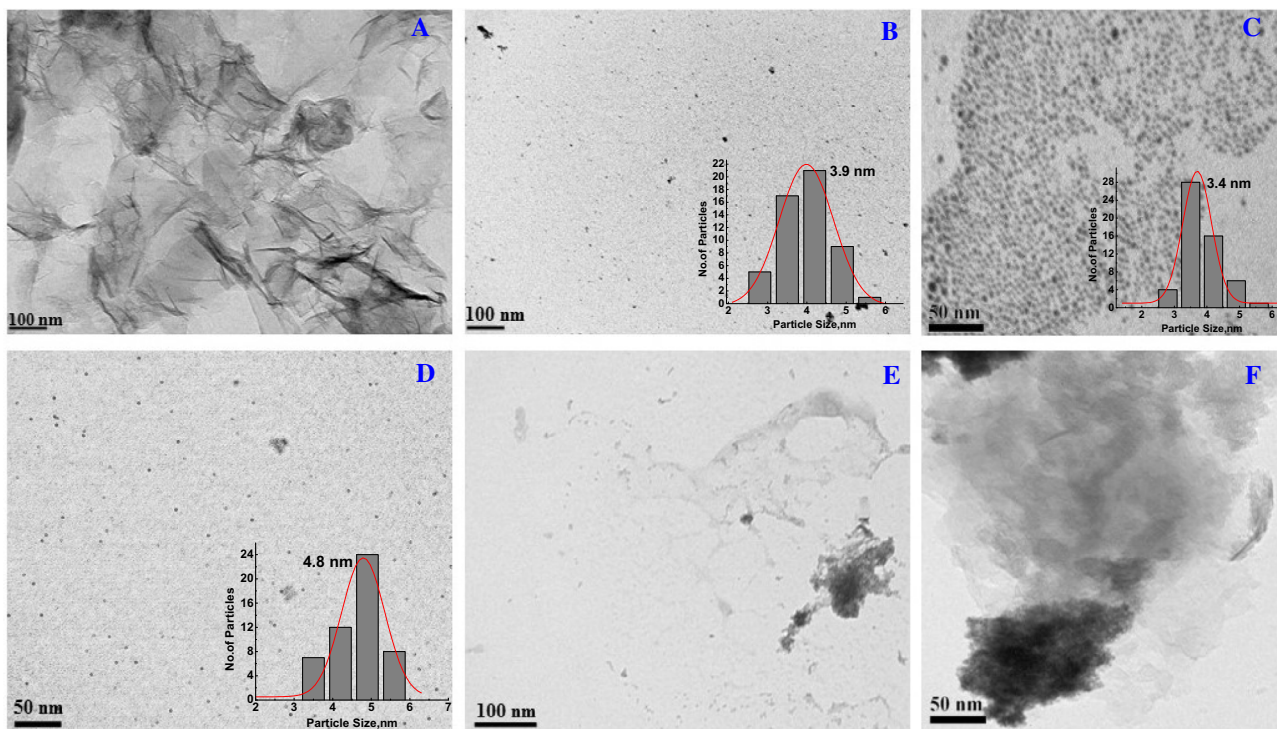


Fig. 3 TEM images of the as-prepared (A) rGO, (B) CeO₂, (C) CdS, (D) CdS/CeO₂ and (E) and (F) CdS/rGO/CeO₂ nanoheterostructure.

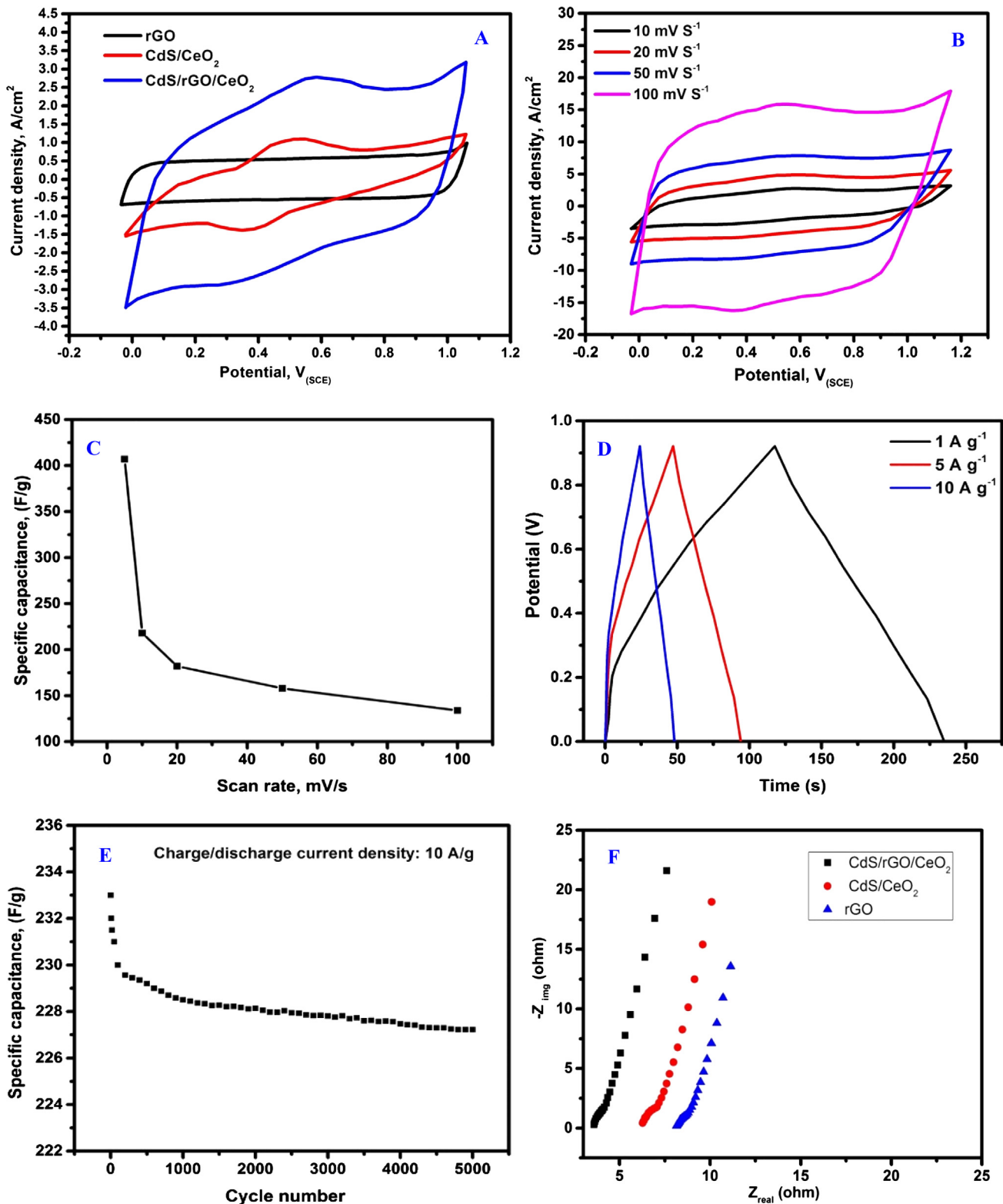


Fig. 4 Electrochemical performance of the CdS/rGO/CeO₂ nanoheterostructure measured in 2 M KOH solution at room temperature. (A) CV curves of the rGO, CdS/CeO₂ and CdS/rGO/CeO₂ electrodes measured at a scan rate of 10 mV s⁻¹, (B) CV curves of CdS/rGO/CeO₂ at different scan rates, (C) plots of the scan rate versus the specific capacitance of the CdS/rGO/CeO₂ electrode, (D) charge/discharge curves at different current densities, (E) cycling performance of the CdS/rGO/CeO₂ electrode at a current density of 10 A g⁻¹ and (F) Nyquist plots of the rGO, CdS/CeO₂ and CdS/rGO/CeO₂ electrodes.

increased the electron transfer and also the peak current between the electrode and the investigated compound (Lei et al., 2014). Obtaining one pair of redox peaks in cyclic voltammetric curve confirms that the capacitance behavior of CdS/rGO/CeO₂ is typical pseudocapacitance. By increasing the scan rate, CV curves for CdS/rGO/CeO₂ nanoheterostructure maintained its shape emphasizing the good capacitive behavior and reversibility and hence the electrochemical stability (Fig. 4B). The specific capacitance (C , in $F\ g^{-1}$) of the electrode was calculated using cyclic voltammetry according to the following equation:

$$C = \left(\int Idt \right) / m\Delta V \quad (2)$$

where I is the response current density (A), dt is the time differential, m is the mass of the CdS/rGO/CeO₂ electrode material and ΔV is the voltage range of one sweep segment (Wang et al., 2011).

Fig. 4C showed the relation between the specific capacitance of the CdS/rGO/CeO₂ nanoheterostructure and the scan rate. From this figure it is clear that increasing the scan rate (5–100 $mV\ s^{-1}$) resulted in decreasing the calculated specific capacitance. Different factors affect the specific capacitance value such as the diffusion of ion in the electrolyte, the adsorption of ions on the electrode surface and the ability to charge transfer in the studied electrode material (Deng et al., 2017).

In our case, decreasing the capacitance with increasing the scan rate explained with the insufficient electrolyte ions limited by the diffusion and time constraints and in this case the charge storage will be performed using the ions of outer active surface only. While at low scan rate, the charge storage increases due to the diffusion of the electrolyte ions into the electrode surface using all the active site for charge storage and hence the specific capacitance increases. From the results obtained, the highest specific capacitance achieved for CdS/rGO/CeO₂ electrode at scan rate 5 $mV\ S^{-1}$ was found to be 407 $F\ g^{-1}$.

Improving the electrochemical performance of CdS/rGO/CeO₂ nanoheterostructure is related to its unique structure due to the improved conductivity of CdS and CeO₂ and the good utilization of graphene which facilitate the electron transport through its conductive network (Deng et al., 2017). Also the good dispersion of the nanoparticles of CdS and CeO₂ in rGO pronouncedly enhances the diffusion of electrolyte ions without significant loss or recombination. As shown in Fig. 4, the value of specific capacitance was constant at 134 $F\ g^{-1}$ after increasing the scan rate up to 100 mV/s . The specific capacitance obtained using the investigated nanoheterostructure was found to be higher than the reported values for different graphene based nanoheterostructure at the same conditions (Saravanan et al., 2015; Chen and Xue, 2015; Dezfouli et al., 2015). The electrochemical capacitance of CdS/rGO/CeO₂ electrode was also calculated using galvanostatic charge-discharge measurements at current densities of 1, 5, 10 A/g as depicted in Fig. 4D. The charge-discharge curves showed the same behavior indicating its electrochemical reversibility. Due to the pseudocapacitance behavior of the CdS/rGO/CeO₂ nanoheterostructure, nonlinear discharge curve was obtained from the redox reaction at electrode-electrolyte interface (Peng et al., 2011).

The specific capacitances calculated using the equation reported elsewhere (Nagamuthu et al., 2013) are 407, 280

and 233 F/g at the current density of 1, 5, 10 A/g, respectively. The results confirm that the capacitance is still high even after increasing the applied current. The enhanced specific capacitance of CdS/rGO/CeO₂ could be attributed to the better conductivity of CdS/rGO/CeO₂ due to the presence of rGO in the heterostructure. Studying the cyclic stability is an important measurement for supercapacitor materials. Fig. 4E depicted the effect of the continuous galvanostatic charge-discharge for the CdS/rGO/CeO₂ architecture on the specific capacitance for 5000 cycles at current density of 10 A/g. From this figure it is obvious that the CdS/rGO/CeO₂ retains about 96% of its initial values after 5000 cycles. CdS/rGO/CeO₂ electrode showed large specific capacitance, high stability and reversibility which might help in the development of a promising supercapacitor.

The electrochemical impedance spectroscopy (EIS) technique was used to understand the reason for the significant electrochemical behavior of the CdS/rGO/CeO₂ nanoheterostructure compared with CdS/CeO₂, in the frequency range from 0.01 Hz to 100 kHz. Fig. 4F, shows Nyquist plots of rGO alone and the investigated nanoheterostructure in 2 M KOH solution. From this figure it is clear that all curves in the low frequency region contain a straight line resulting from Warburg impedance while in the high frequency region a semicircle was obtained resulting from the resistance and capacitance.

In comparison, CdS/rGO/CeO₂ heterostructure showed EIS plot with vertical slope higher than the plot obtained in case of CdS/CeO₂ heterostructure or rGO at low frequency, illustrating the highest capacitive behavior of CdS/rGO/CeO₂ heterostructure and the lower diffusion resistance of electrolyte ions in the electrode compared with CdS/CeO₂ or rGO, which agreed well with the cyclic voltammetric data. Also from EIS plot it is clear that the CdS/rGO/CeO₂ showed shorter semicircles radius at the high frequency region compared with CdS/CeO₂ or rGO, which means decreasing the charge transfer resistance on the electrode surface and hence increasing interfacial electron transfer which suggests great conductivity for ion transport resulting from the presence of graphene which has excellent conductivity (Ye et al., 2015).

4. Conclusion

In summary, we have successfully fabricated a CdS/rGO/CeO₂ nanoheterostructure via a hydrothermal method. The investigated nanoheterostructure showed a well-distributed particle size and exhibited excellent electrochemical performance, such as excellent cycling stability, and good reversibility and stability which are critical factors in practical applications for supercapacitors. The investigated nanoheterostructure showed high specific capacitance of 407 F/g with retention of about 96% of the initial value even after 5000 charge-discharge cycles. The results confirmed that the prepared electrode material may be used in a wide range of energy storage applications.

Acknowledgements

We would like to gratefully acknowledge the support of Kuwait University, research sector, Project No. SC 10/16 and SAF Facilities No. (GS 03/01 and GS 01/05). Also, the

support provided by the nanoscopy science centre at Kuwait University is highly acknowledged.

References

- Bumajdad, A., Zaki, M.I., Eastoe, J., Pasupulety, L., 2006. Characterization of nano-cerias synthesized in microemulsions by N₂ sorptiometry and electron microscopy. *J. Colloid Interface Sci.* 302 (2), 501–508.
- Bumajdad, A., Eastoe, J., Mathew, A., 2009. Cerium oxide nanoparticles prepared in self-assembled systems. *Adv. Colloid Interface Sci.* 147–148 (Supplement C), 56–66.
- Cao, A., Liu, Z., Chu, S., Wu, M., Ye, Z., Cai, Z., Chang, Y., Wang, S., Gong, Q., Liu, Y., 2010. *Adv. Mater.* 22, 103.
- Chen, W.C., Hu, C.C., Wang, C.C., Min, C.K., 2004. *J. Power Sources* 125, 292.
- Chen, K., Xue, D., 2015. In-situ electrochemical route to aerogel electrode materials of grapheme and hexagonal CeO₂. *J. Colloid Interface Sci.* 446, 77–83.
- Chen, Y., Zhang, X., Zhang, H., Sun, X., Zhang, D., Ma, Y., 2012. High-performance supercapacitors based on a graphene-activated carbon composite prepared by chemical activation. *RSC Adv.* 2, 7747–7753.
- Deng, D., Chen, N., Li, Y., Xing, X., Liu, X., Xiao, X., Wang, Y., 2017. *Phys. E: Low-Dimension. Syst. Nanostruct.* 86, 284–291.
- Dezfuli, A.S., Ganjali, M.R., Naderi, H.R., Norouzi, P., 2015. A high performance supercapacitor based on a ceria/graphene nanocomposite synthesized by a facile sonochemical method. *RSC Adv.* 5, 46050–46058.
- Frackowiak, E., 2007. Carbon materials for supercapacitor application. *Phys. Chem. Chem. Phys.* 9, 1774–1785.
- Han, G., Liu, Y., Zhang, L., Kan, E., Zhang, S., Tang, J., Tang, W., 2014. MnO₂ nanorods intercalating graphene oxide/polyaniline ternary composites for robust high-performance supercapacitors. *Sci. Rep.* 4, 4824–4830.
- Huang, M., Zhao, X.L., Li, F., Li, W., Zhang, B., Zhang, Y.X., 2015. Synthesis of Co₃O₄/SnO₂@MnO₂ core-shell nanostructures for high-performance supercapacitors. *J. Mater. Chem. A* 3, 12852–12857.
- Hummers Jr., W.S., Offeman, R.E., 1958. *J. Am. Chem. Soc.* 80 (6), 1339.
- Jing, D., Guo, L., 2007. Efficient hydrogen production by a composite CdS/mesoporous zirconium titanium phosphate photocatalyst under visible light. *J. Phys. Chem. C* 111, 13437–13441.
- Kalubarme, R.S., Kim, Y.H., Park, C.J., 2013. One step hydrothermal synthesis of a carbon nanotube/cerium oxide nanocomposite and its electrochemical properties. *Nanotechnology* 24, 365401–365408.
- Kumar, S., Ojha, A.K., Patrice, D., Yadav, B.S., Materny, A., 2016. One-step in situ synthesis of CeO₂ nanoparticles grown on reduced graphene oxide as an excellent fluorescent and photocatalyst material under sunlight irradiation. *PCCP* 18 (16), 11157–11167.
- Lei, Y., Li, R., Chen, F., Xu, J., 2014. Hydrothermal synthesis of graphene–CdS composites with improved photoelectric characteristics. *J. Mater. Sci: Mater. Electron* 25, 3057–3061.
- Li, X., Song, H., Wang, H., Zhang, Y., Du, K., Li, H., Huang, J., 2012. A nanocomposite of graphene/MnO₂ nanoplatelets for high-capacity lithium storage. *J. Appl. Electrochem.* 42, 1065–1070.
- Li, L., Zhang, X., Qiu, J., Weeks, B.L., Wang, S., 2013. Reduced graphene oxide-linked stacked polymer forests for high energy-density supercapacitor. *Nano Energy* 2, 628–635.
- Liang, R., Cao, H., Qian, D., Zhang, J., Qu, M., 2011. *J. Mater. Chem.* 21, 17654.
- Miller, J.R., Simon, P., 2008. Electrochemical capacitors for energy management. *Science* 321, 651–652.
- Nagamuthu, S., Vijayakumar, S., Muralidharan, G., 2013. Synthesis of Mn₃O₄/amorphous carbon nanoparticles as electrode material for high performance supercapacitor applications. *Energy Fuel* 27, 3508–3515.
- Peng, X.Y., Liu, X.X., Diamond, D., Lau, K.T., 2011. Synthesis of electrochemically-reduced graphene oxide film with controllable size and thickness and its use in super-capacitor. *Carbon* 49, 3488.
- Primo, A., Marino, T., Corma, A., Molinari, R., Garcia, H., 2011. Efficient visible-light photocatalytic water splitting by minute amounts of gold supported on nanoparticulate CeO₂ obtained by a biopolymer templating method. *J. Am. Chem. Soc.* 43, 123–125.
- Sankar, K.V., Selvan, R.K., 2015. The ternary MnFe₂O₄/graphene/polyaniline hybrid composite as negative electrode for supercapacitors. *J. Power Sources* 275, 399–407.
- Saravanan, T., Shanmugam, M., Anandan, P., Azhagurajan, M., Pazhanivel, K., Arivanandhan, M., Hayakawad, Y., Jayavel, R., 2015. Facile synthesis of graphene-CeO₂ nanocomposites with enhanced electrochemical properties for supercapacitors. *Dalton Trans.* 44, 9901–9908.
- Shan, W., Liu, F., He, H., Shi, X., Zhang, C., 2012. *Catal. Today* 184, 160–165.
- Some, S., Ho, S.-M., Dua, P., Hwang, E., Shin, Y.H., Yoo, H.J., Kang, J.-S., Lee, D.-K., Lee, H., 2012. Dual functions of highly potent graphene derivative poly-L-lysine composites to inhibit bacteria and support human cells. *ACS Nano* 6, 7151–7161.
- Su, Q., Chang, L., Zhang, J., Du, G., Xu, B., 2013. In situ TEM observation of the electrochemical process of individual CeO₂/Graphene anode for lithium ion battery. *J. Phys. Chem. C* 117, 4292–4298.
- Wang, Y.G., Li, B., Cui, L.F., Kang, S.F., Li, X., Zhou, L.H., 2013. *Appl. Catal. B: Environ.* 130–131, 277–284.
- Wang, Y., Shi, R., Lin, J., Zhu, Y., 2010. *Appl. Catal., B* 100, 179.
- Wang, Y., Guo, C.X., Liu, J., Chen, T., Yang, H., Li, C.M., 2011. CeO₂ nanoparticles/graphene nanocomposite-based high performance supercapacitor. *Dalton Trans.* 40, 6388–6391.
- Wang, Z., Wang, Q., Liao, Y., Shen, G., Gong, X., Han, N., Liu, H., Chen, Y., 2011. *ChemPhysChem* 12, 2763–2770.
- Wang, Y., Wang, F., He, J., 2013. *Nanoscale* 5, 11291.
- Xue, T., Xu, C.L., Zhao, D.D., Li, X.H., Li, H.L., 2007. *J. Power Sources* 164, 953.
- Yang, T.T., Chen, W.T., Hsu, Y.J., Wei, K.H., Lin, T.Y., Lin, T.W., 2010. *J. Phys. Chem. C* 114, 11414.
- Yang, Z., Huang, G., Huang, W., Wei, J., Yan, X., Liu, Y., Jiao, C., Wan, Z., Pan, A., 2014. Novel Ag₃PO₄/CeO₂ composite with high efficiency and stability for photocatalytic applications. *J. Mater. Chem. A* 2, 1750–1756.
- Ye, G., Gong, Y., Keyshar, K., Husain, E.A.M., Brunetto, G., Yang, S., Vajtai, R., Ajayan, P.M., 2015. 3D reduced graphene oxide coated V₂O₅ nanoribbon scaffolds for high-capacity supercapacitor electrodes part. *Part. Syst. Charact.* 32, 817–821.
- You, D., Pan, B., Jiang, F., Zhou, Y., Su, W., 2016. CdS nanoparticles/CeO₂ nanorods composite with high-efficiency visible-light-driven photocatalytic activity. *Appl. Surf. Sci.* 363, 154–160.
- Zhang, X., Ge, X., Sun, S., Qu, Y., Chi, W., Chen, C., Lü, W., 2016. Morphological control of RGO/CdS hydrogels for energy storage. *Cryst. Eng. Comm.* 18, 1090–1095.
- Zhang, H., Zhu, Y.F., 2010. *J. Phys. Chem. C* 114, 5822.
- Zhao, W., Bai, Z., Ren, A., Guo, B., Wu, C., 2010. Sunlight photocatalytic activity of CdS modified TiO₂ loaded on activated carbon fibers. *Appl. Surf. Sci.* 256, 3493–3498.